Results in Physics 17 (2020) 103059

Contents lists available at ScienceDirect

Results in Physics

journal homepage: www.elsevier.com/locate/rinp

Morphological, structural and optical behaviour of PVA capped binary $(NiO)_{0.5}$ $(Cr_2O_3)_{0.5}$ nanoparticles produced via single step based thermal technique

Naif Mohammed Al-Hada[a,b,c,*], Halimah Mohamed Kamari[d,*], Muneer Aziz Saleh[b], Moayad Husein Flaifel[e,f], Abbas M. Al-Ghaili[g], Hairoladenan Kasim[h], Anwar Ali Baqer[i], Elias Saion[d], Wang Jihua[a,*]

[a] Shandong Key Laboratory of Biophysics, Institute of Biophysics, Dezhou University, Dezhou 253023, China
[b] Nuclear Engineering Programme, School of Chemical and Energy Engineering, Universiti Teknologi Malaysia, 81310 Skudai, Johore Bahru, Johore, Malaysia
[c] Department of Physics, Faculty of Applied Science, Thamar University, Dhamar 87246, Yemen
[d] Department of Physics, Faculty of Science, Universiti Putra Malaysia, 43400 Serdang, Selangor, Malaysia
[e] Department of Physics, College of Science, Imam Abdulrahman Bin Faisal University, P.O. Box 1982, 31441 Dammam, Saudi Arabia
[f] Basic and Applied Scientific Research Center, College of Science, Imam Abdulrahman Bin Faisal University, P.O. Box 1982, 31441 Dammam, Saudi Arabia
[g] Institute of Informatics and Computing in Energy (IICE), Universiti Tenaga Nasional (UNITEN), 43000 Kajang, Selangor, Malaysia
[h] College of Computing & Informatics (CCI), UNITEN, 43000 Kajang, Selangor, Malaysia
[i] Department of Physics, Faculty of Science for Women, University of Baghdad, 10071 Baghdad, Iraq

ARTICLE INFO

Keywords:
Thermal treatment
Polyvinyl alcohol PVA
Binary metal oxide
Semiconductor nanoparticles
Energy applications

ABSTRACT

In this research study, a thermal treatment approach based on a novel single-step has been utilised to addresses the synthesis of binary $(NiO)_{0.5}$ $(Cr_2O_3)_{0.5}$ nanoparticles. Characteristics of these binary metal oxide nanoparticles were examined by employing appropriate characterization tools. Sample patterns of X-ray diffractions were used, calcined with temperature (*Temp*), set to 500 °C revealed the existence of face-centred cubic (fcc) and hexagonal crystalline structures (hcs). It was noted that with a rising calcination temperature, the nanoparticle dispersal was enhanced further. On the other hand, TEM micrographs have been used to calculate the size of the mean particle. It was found that there was a rising tendency with the increased calcination temperature and this the growth of the mean particle. Increased particle size inherited a rise of nanoparticles' photoluminescence intensity, as suggested by recorded spectra, and various energy band gaps. This result would have been reduced as an effect once calcination temperature was increased. Resulting $(NiO)_{0.5}$ $(Cr_2O_3)_{0.5}$ nanoparticles could be used in the realm of semiconductors and energy applications.

Introduction

Recently, there has been a remarkable growth in the research activities of nanomaterials arena has been observed. Amongst which, semiconductor nanomaterials with intriguing optoelectronic and catalytic properties are deemed of great interest because of their potential role in a wide range of applications [1–4]. Of these, nano-sized nickel oxide (NiO), with its rock salt simple structure, is considered a significant p-type metal oxide semiconductor with a band gap equal to 3.6 − 4.0 eV and excellent chemical stability [5,6], It has been utilised in several applications including chemical and gas sensing, solar cells, optoelectronic devices, and waste water treatment [7–11]. Another metal oxide of interest is chromium (III) oxide (Cr_2O_3), which is famously known as eskolaite or chromia. It is a p-type metal oxide semiconductor, having a hexagonal structure and distinct properties such as high melting point, excellent corrosion resistance and promising electrical conductivity. Furthermore, recording have shown that the direct energy band gap equals approximately 3.00 eV and indirect energy band gap approximately equals to 3.40 eV [12]. These interesting properties, which are further enhanced in its nanostructure, allow chromia to be involved in many beneficial applications including solar photovoltaic cells, chemical and gas sensing, and biomedical applications [12–15].

Binary material related studies involve a mixture of two phases

* Corresponding authors at: Shandong Key Laboratory of Biophysics, Institute of Biophysics, Dezhou University, Dezhou 253023, China (N.M. Al-Hada and W. Jihua); Universiti Putra Malaysia, Serdang 43400, Malaysia (H.M. Kamari).
E-mail addresses: naifalhada@yahoo.com (N.M. Al-Hada), hmk6360@gmail.com (H.M. Kamari), jhw25336@126.com (W. Jihua).

https://doi.org/10.1016/j.rinp.2020.103059
Received 6 February 2020; Received in revised form 8 March 2020; Accepted 12 March 2020
Available online 13 March 2020

possessing dissimilar chemical compositions. These appealing properties stemmed from combining two different metal oxides in nanometric size as the driving forces behind the continuous research into the realm of binary metal oxide semiconductor materials [16–18]. Since both NiO and Cr_2O_3 share similar properties clearly observed from their ionic radii (0.70 Å for Ni^{+2} and 0.63 Å for Cr_2O_3) and bad gap energies [5], it is considered that consolidating these aspects would make it likely to see a rise in associated functionality, to a level greater than what could be attained through their individual forms [19].

A number of techniques addressed in literature were used to synthesise metal oxide semiconductor nanomaterial e.g., co-precipitation [20], sol-gel [21], thermal decomposition [22], microwave irradiation [23], precipitation [24], sonochemical [25], electrochemical [26], and wet chemical methods [27,28]. Besides the high cost and low yielding drawbacks associated with most of the aforementioned synthesis methods used to produce metal oxide semiconductor nanomaterials, these methods exhibit difficulties pertaining the sophisticated procedures at commercial scale production. In addition, there is the problem of poisonous byproducts and toxic reagents being released during the synthesis process, which cause environmental pollution. Thus, a different approach is deemed necessary. Other techniques proposed in Refs. [29–34] have produced metal oxide nanostructures with cost effective, eco-friendly and antibacterial activity against many Gram positive and Gram negative bacterial pathogens. There are research works carried out to produce binary metal oxide nanoparticles, and the thermal treatment technique was one of the implemented approaches deemed simple, less expensive, environmentally friendly, and proven to provide consistent and high quality metal oxide semiconductor nanomaterials [35–51]. However, there is no report available that discusses the synthesis of binary $(NiO)_x$ $(Cr_2O_3)_{1-x}$ using thermal treatment method. Therefore, in this work a single step based novel method is employed to synthesise binary $(NiO)_{0.5}$ $(Cr_2O_3)_{0.5}$ nanoparticles involving the heat treatment approach. The effectiveness of the capping agent used in this technique was described. The effect of structural, morphological and optical characteristics of $(NiO)_{0.5}$ $(Cr_2O_3)_{0.5}$ nanoparticles caused by different calcination temperatures was also investigated in detail.

Experimental method

Materials

In this experiment research, the Nickel (II) acetate tetrahydrate $Ni(OCOCH_3)_2{\cdot}4H_2O$ (M_W = 248.84 g/mol) and Chromium (III) acetate hydrate $Cr_2(CH_3CO_2)_4{\cdot}2(H_2O)$ (M_W = 247.143 g/mol) had been used as metal precursors, polyvinyl alcohol (PVA) had been employed to be a capping agent to attempt to disperse the particles, and deionized water had been employed to be a solvent. $Ni(OCOCH_3)_2{\cdot}4H_2O$ (99%), $Cr_2(CH_3CO_2)_4{\cdot}2(H_2O)$ (99%) and PVA (MW = 61,000) had been attained with the help of Sigma-Aldrich.

Methodology

In this technique, 0.5 mmol of $Ni(OCOCH_3)_2{\cdot}4H_2O$ was dissolved, and then 0.5 mmol of $Cr_2(CH_3CO_2)_4{\cdot}2(H_2O)$ and 4% of PVA had been added, before being mixed rigorously until a homogeneous solution had been formed. The petri dish has been employed to receive the obtained solution result, in order to dry at temp of 80 °C for 24 h. Afterwards, a dry sample with a yellow colour was attained and then grained, where some had retained a room temp = 27–30 °C to examine the purposes via XRD and FTIR. The remaining portion was divided into four parts. For calcination purposes, four temperature variations were adopted, each of which took 3 h. The temperature were temp = 500, 600, 700, and 800 °C, respectively.

Characterisation

Numerous characterisation methods were used to study the sample prepared by the thermal path. For the samples' crystalline structure to be examined, an X-ray diffractometer (Shimadzu 6000 model) was used at an ambient temperature in 2θ, set to be between twenty and eighty degrees, while Cu Kα (0.154 nm) was the source of radiation. An EDX spectroscopy had been performed using an EDX spectrometer (7353 model, Oxford Instruments, UK), after samples had been sputter-coated with gold. Transmission electron microscopy was also utilised (JEOL TEM 2010F UHR model) to accelerate voltage of 200 kV in order to assess the nanopowders' morphology dimension distribution and consistency. A Fourier transform infrared (FTIR) spectrometer (Perkin Elmer 1650 model) using KBr was employed to assess samples' infrared spectra ranging between 280 cm^{-1} and 4000 cm^{-1}. Thus, inorganic sample's post-calcination presence in its composite form could be assessed. Further, capping agent removal could be seen as possibility of confirmation. The samples' optical characteristics have been well studied at ambient temperatures ranging from two-hundred to eight-hundred nm using a UV–vis spectrophotometer (Shimadzu UV-3600 model), as well as using measurement of photoluminescence (PL) performed at room temperature through a spectrofluorometer equipped with a Xenon lamp (LS-55 Perkin Elmer model).

Results and discussion

Analysis of XRD

X-ray diffractograms of the prepared $(NiO)_{0.5}$ $(Cr_2O_3)_{0.5}$ nanopowder before and after calcination are shown in Fig. 1. It can be recognized that the sample before calcination exhibits no trace of typical diffraction peaks, suggesting its amorphous behavior. On the other hand, the crystalline behavior of $(NiO)_{0.5}$ $(Cr_2O_3)_{0.5}$ nanopowder can be seen clearly after it has been calcined at different temperature values of 500, 600, 700 and 800 °C. The diffraction peaks appearing in the XRD pattern are typical values which correspond to NiO and Cr_2O_3 nanoparticles with face centered cubic and hexagonal structures, respectively. As per the JCPDS Card 36-1451, the diffraction peaks of NiO nanoparticles are well indexed to (1 1 1), (2 0 0), (2 2 0) and (3 1 1) planes [52]. Similarly, according to the JCPDS Card 38-1479, the diffraction peaks of Cr_2O_3 are linked to (0 1 2), (1 0 4), (1 1 0), (0 0 6), (1 1 3), (0 2 4), (2 1 1), (0 1 8), (2 1 4), (0 3 0), (2 1 1), (0 1 0) and (2 2 0) planes [12]. These phases co-exist due to separate grains of NiO and Cr_2O_3. The phases configuration was obtained this way because the two systems are stable as in the case of chemically stable systems [53,54].

The crystallites' average size of nanoparticles has been calculated (as shown in Table 1) in accordance to the well known formula of Debye-Scherrer [55]:

$$D = \frac{k.\lambda}{\beta.\cos\theta} \quad (1)$$

where

- D is crystallites average size
- k is shape factor = 0.9
- λ is the X-ray wavelength corresponding to Cu Kα = 0.154 nm
- β is the full width at half of the maximum intensity peak measured in radians (FWHM)
- θ is the Bragg's diffraction angle refers to the peak position [56].

From the results, and as can be seen in Fig. 1(b)–(e), the diffraction peaks became sharper and narrower with higher intensities as a result of the increasing calcination temperature. Thus, the crystallinity of binary nanopowders has significantly been enhanced with calcination temperatures.

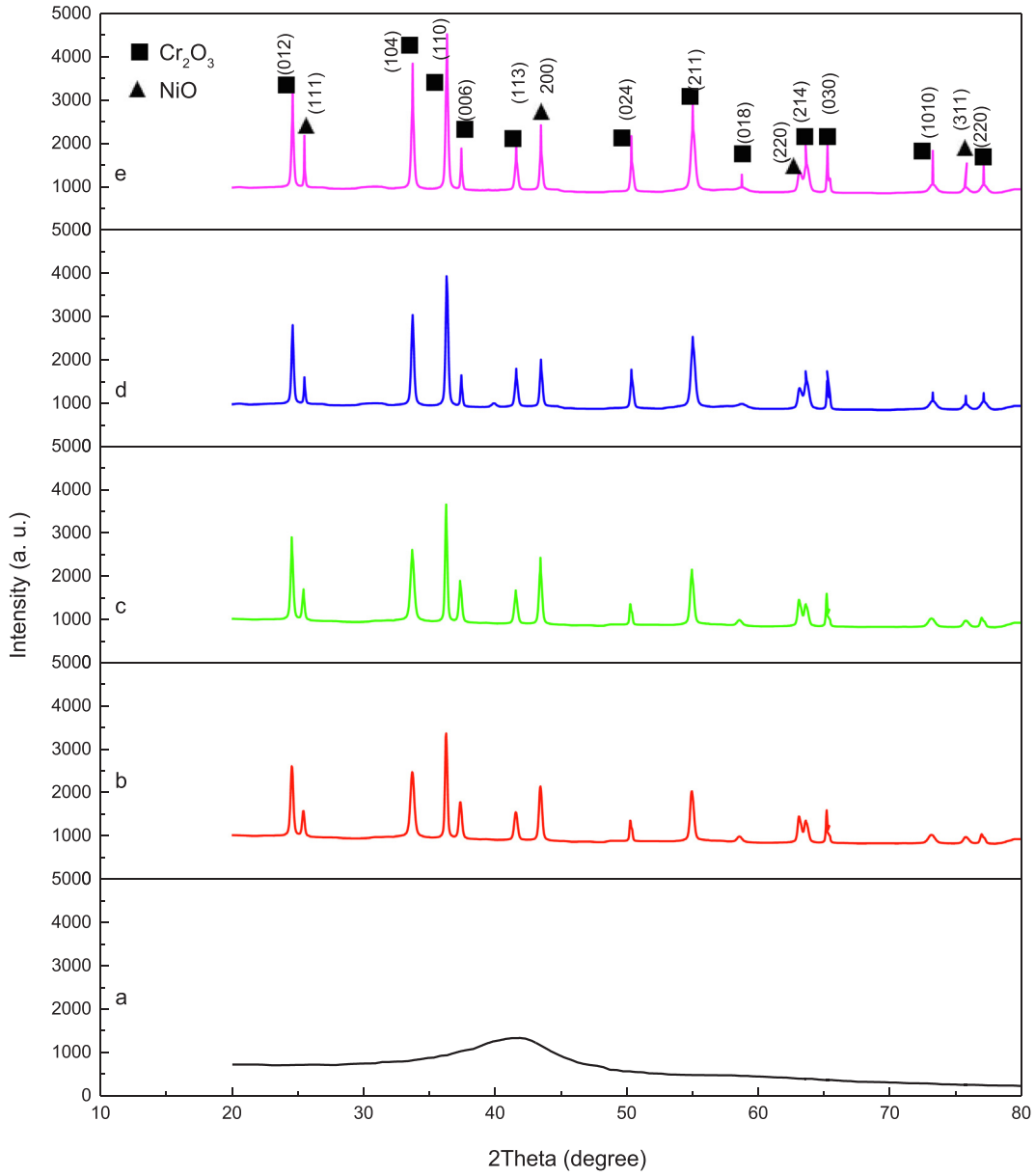

Fig. 1. XRD patterns of binary $(NiO)_{0.5}$ $(Cr_2O_3)_{0.5}$ nanoparticles prepared at (a) room temperature of 30 °C, and at different calcination temperatures of (b) 500, (c) 600, (d) 700 and (e) 800 °C.

Table 1
XRD and TEM data for the binary oxide nanoparticles at various temperatures.

Calcination temperature (°C)	Crystal size, D_{XRD} (nm)	Particle size, D_{TEM} (nm)
500	8.6	9 ± 3
600	13.4	14 ± 4
700	17.9	19 ± 3
800	31.8	33 ± 5

Morphological & size distribution analysis using TEM

Fig. 2(a)–(d) display the TEM results of prepared samples of $(NiO)_{0.5}$ $(Cr_2O_3)_{0.5}$ nanopowders that were calcined at different temperature variations. From these images, the morphology of the synthesized binary nanoparticles is recognized to possess a uniform spherical shape for all calcined samples. Moreover, size of particle increased remarkably with calcination temperature increases as shown in Table 1. This is explained through the fact that the small crystallites of each particle have expanded at higher temperatures and hence coalesce with that of the other particles, thus forming larger particles.

Another point worth mentioning is the homogeneous dispersion of $(NiO)_{0.5}$ $(Cr_2O_3)_{0.5}$ nanoparticles observed for all calcination temperature values. This result is essentially credited to the presence of polyvinyl alcohol (PVA) which curbed the nanoparticles' propensity to agglomerate. The aforementioned results emphasise the effectiveness of the adopted preparation technique when it come to producing high quality binary nanoparticles with being homogenously dispersed.

EDX analysis

The initial composition of synthesized binary $(NiO)_{0.5}$ $(Cr_2O_3)_{0.5}$ samples at room temperature calcined at 600 °C, was verified via the EDX spectrum as depicted in Figs. 3(a) and (b). The sample shown in Fig. 3(a) at room temperature has indicated that all compositions appeared. For the calcined sample at 600 °C, the presence of elements Ni, Cr and O can be noticeably obvious as for the sample shown in Fig. 3(b). It is clearly seen that the spectrum ascertains the presence of $(NiO)_{0.5}$

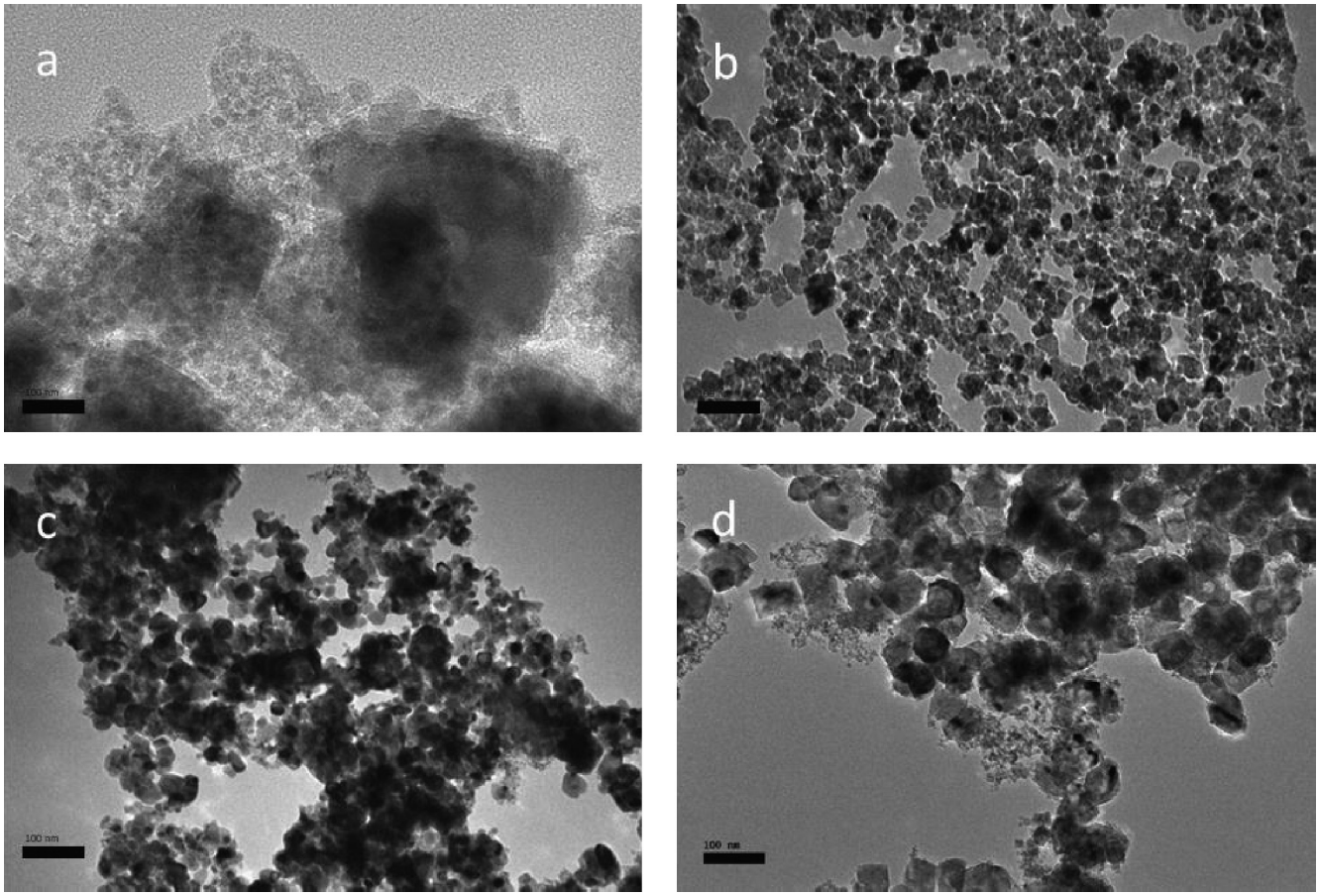

Fig. 2. TEM images and particle size distribution of $(NiO)_{0.5}$ $(Cr_2O_3)_{0.5}$ nanoparticles at calcination temperatures of (a) 500 (b) 600, (c) 700 and (d) 800 °C.

$(Cr_2O_3)_{0.5}$ nanoparticles in terms of the existing peaks corresponding to the individual elemental constituents i.e. Ni, Cr and O. Other peaks noticed in the spectrum are related to the gold used for the analysis. It has have been consumed in the sputter- coating process of nanoparticles, in order to avoid undesired electrostatic charging and to improve secondary electron signal received from the nanoparticles' surface [57]. The atomic composition (%) ratio of [Ni:Cr:O] determined from EDX data is [14.3:28.6:57.1] %, which approximately confirms

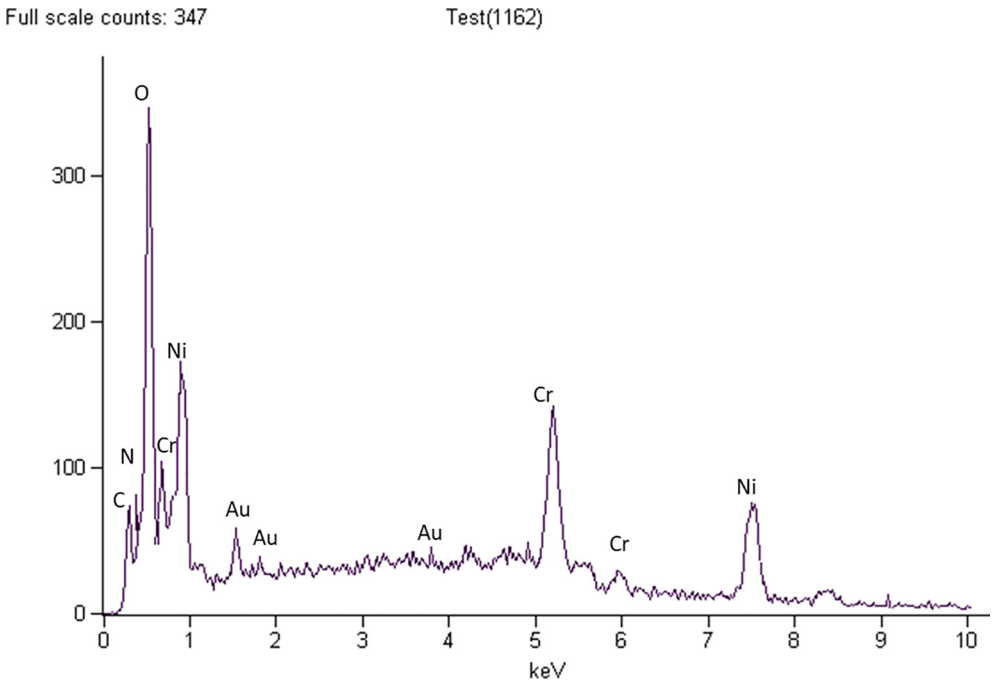

Fig. 3a. EDX spectrum of binary $(NiO)_{0.5}$ $(Cr_2O_3)_{0.5}$ nanoparticles calcined at room temperature.

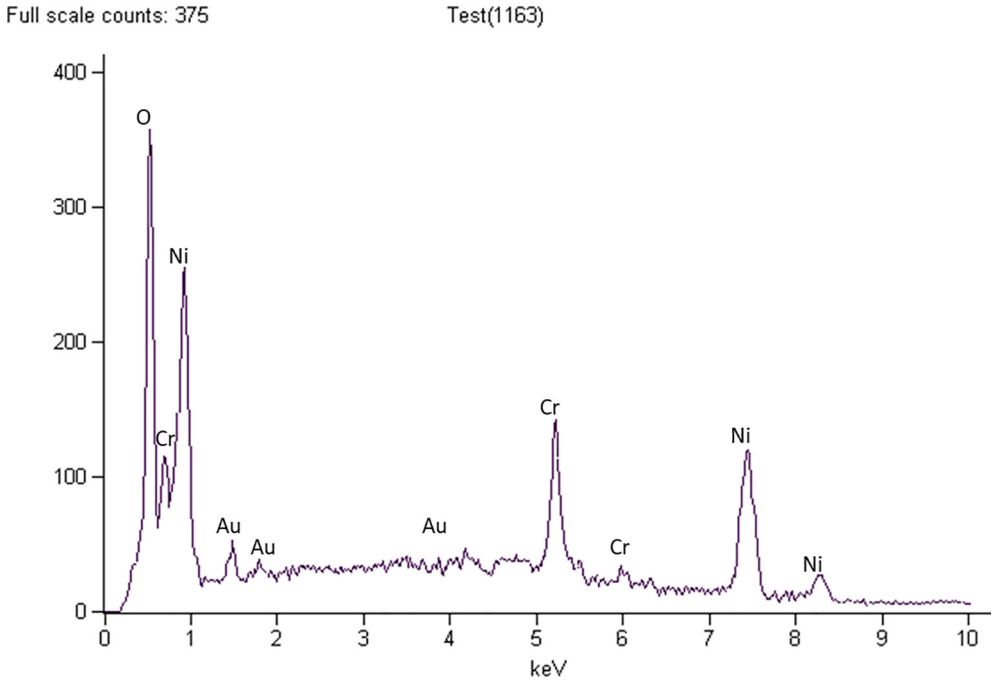

Fig. 3b. EDX spectrum of binary $(NiO)_{0.5}$ $(Cr_2O_3)_{0.5}$ nanoparticles calcined at 600 °C.

the Ni to Cr precursors 5:10 ratio which in turn is revealed by the chemical formula of their nanoparticles compound i.e. $(NiO)_{0.5}$ $(Cr_2O_3)_{0.5}$. Organic compound absence through the adopted synthesis processes is another sign that proves the effectiveness of this approach.

FTIR analysis

As seen in Fig. 4, FTIR spectra related to synthesized $(NiO)_{0.5}$ $(Cr_2O_3)_{0.5}$ nanopowders have been demonstrated before and after calcination, which was conducted at different temperature variations in the range of 280–4500 cm^{-1}. The PVA and bimetal nitrate traces were observed through their distinct absorption peaks. For the as-synthesized sample without calcination, various absorptions peaks took place at wave numbers 3414, 2945, 1646, 1428, 1277, 839, 639, 582 cm^{-1}. Absorption peaks located at 3414, 2945 and 1646 cm^{-1} are attributed to N–H, C–H and C═ O stretching vibrations [52,58,59]. Additionally, the peak noticed at 1428 cm^{-1} was a result of –C–H bending vibration in the methylene group, while the peak was observed at 1277 cm^{-1}.

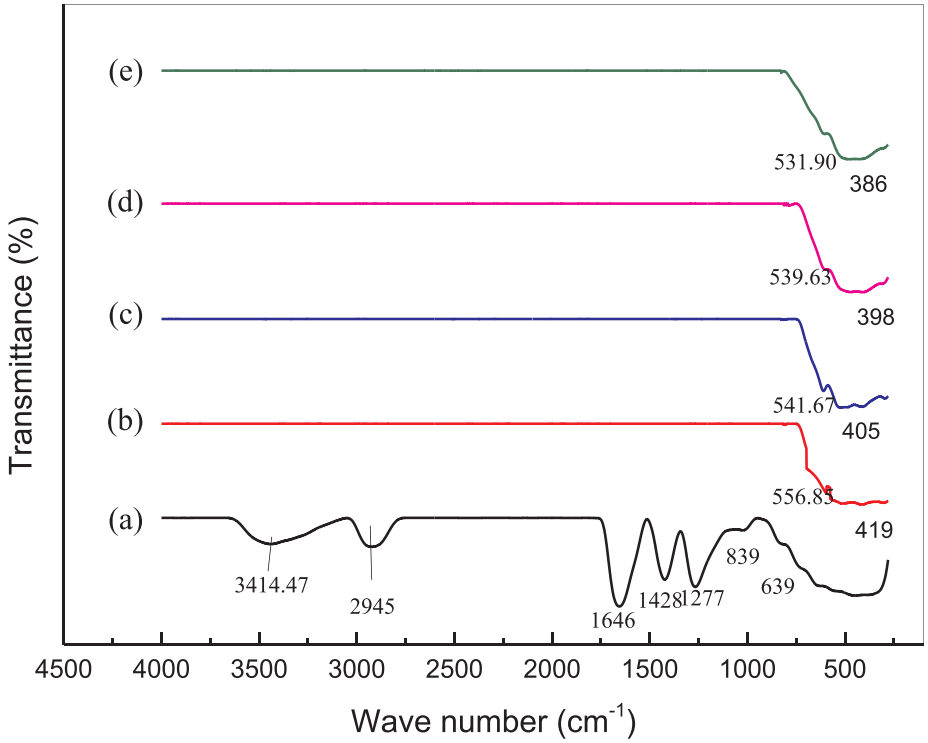

Fig. 4. FTIR of binary $(NiO)_{0.5}$ $(Cr_2O_3)_{0.5}$ nanoparticles prepared at (a) room temperature 30 °C, and at calcination temperatures of (b) 500, (c) 600, (d) 700 and (e) 800 °C.

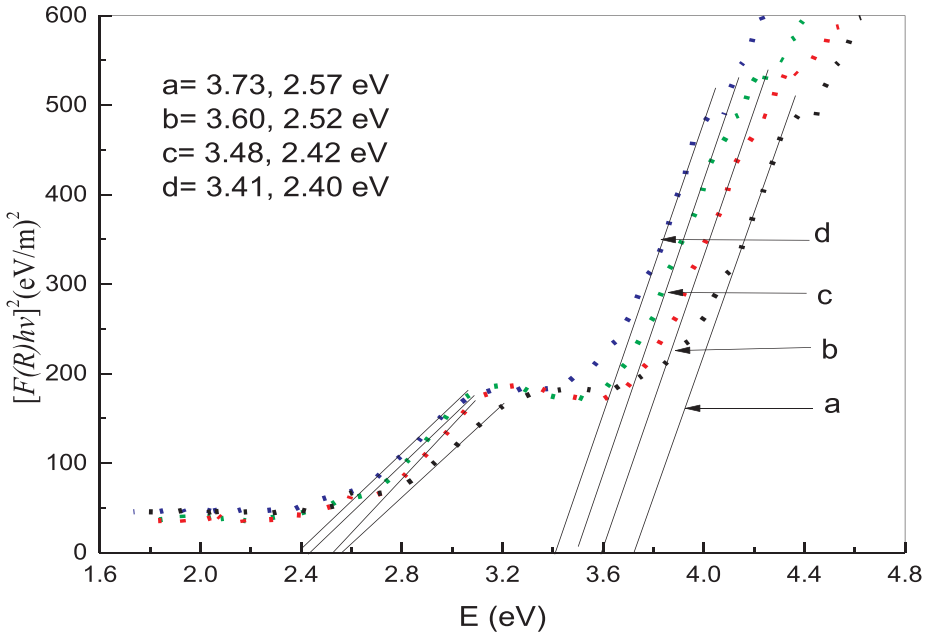

Fig. 5. Energy band gab of $(NiO)_{0.5}$ $(Cr_2O_3)_{0.5}$ nanoparticles at calcination temperatures of (a) 500 (b) 600, (c) 700 and (d) 800 °C.

This peak was ascribed to the C–N stretching vibration. Remaining peaks at 839 and 639 cm^{-1} were a consequence of C–N═O bending vibration in NO_3^- groups [60,61].

For whole calcined samples at various temperatures, there has been an absence of absorption peaks in the corresponding wave number range except for values below 560 cm^{-1}. Two absorption peaks were observed below 560 cm^{-1}, which were seen to move to lower wave number values due to calcination temperature increases. This suggests the formation of highly pure $(NiO)_{0.5}$ $(Cr_2O_3)_{0.5}$ nanoparticles.

UV–vis analysis

The UV–Vis analysis is carried out to study changes of the optical band gap of nanopowders exposed to heat treatment procedures. The obtained diffuse reflectance spectra of the synthesized binary $(NiO)_{0.5}$ $(Cr_2O_3)_{0.5}$ nanopowders, with a range of 220–800 nm in term of wavelength, were transformed using the Kubelka-Munk method as depicted in Fig. 5. Subsequently, the optical band gap values were measured based on transformed spectra using Eq. (2) [62]:

$$(F(R_\infty)\cdot h\nu)^2 = A(h\nu - E_g) \quad (2)$$

Fig. 5 illustrates the transformed reflectance spectra to show the plotted values of $(F(R_\infty)\cdot h\nu)^2$ as a function of $h\nu$ for all $(NiO)_{0.5}$ $(Cr_2O_3)_{0.5}$ nanoparticle samples. Values of optical band gaps of different samples for $(NiO)_{0.5}$ $(Cr_2O_3)_{0.5}$ nanopowders were calculated based on line projections that were extrapolated to intercept the $h\nu$ axis (as provided in Table 2).

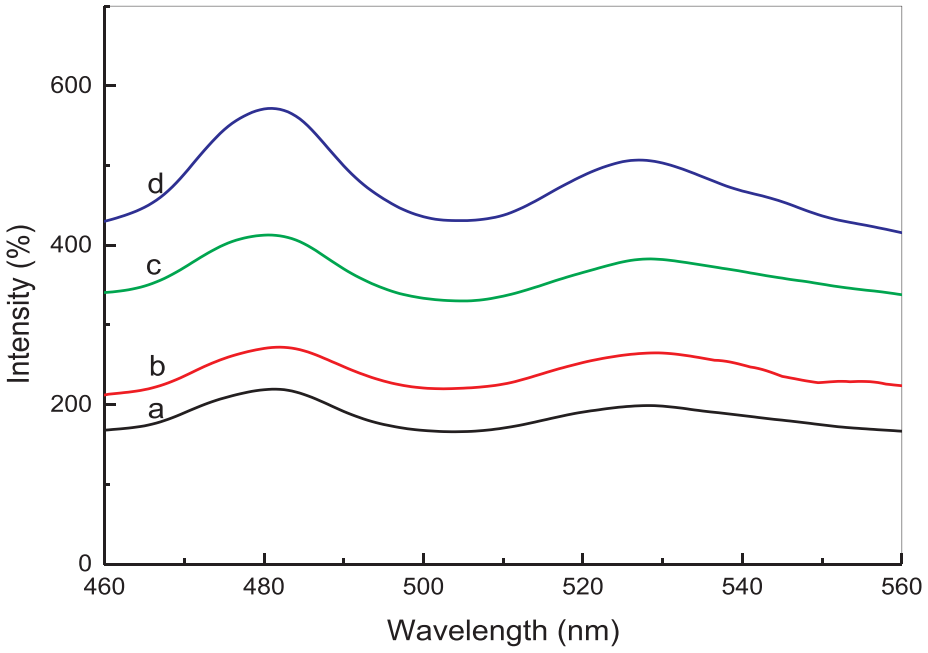

Fig. 6. PL of $(NiO)_{0.5}$ $(Cr_2O_3)_{0.5}$ nanoparticles at calcination temperatures of (a) 500 (b) 600, (c) 700 and (d) 800 °C.

Table 2
Energy band gap data for the binary oxide nanoparticles at various temperatures.

T °C	500	600	700	800
$(NiO)_{0.5}(Cr_2O_3)_{0.5}$ Nanoparticles		Eg (eV)		
$(NiO)_{0.5}$	3.73	3.60	3.48	2.41
$(Cr_2O_3)_{0.5}$	2.57	2.52	2.42	2.40

Table 3
Pl data for the binary oxide nanoparticles at various temperatures.

T °C	500	600	700	800
$(NiO)_{0.5}(Cr_2O_3)_{0.5}$ Nanoparticles		Intensity (%)		
$(NiO)_{0.5}$	197	266	382	506
$(Cr_2O_3)_{0.5}$	215	275	412	571

Photoluminescence analysis (PL)

To investigate the photoluminescence property of the synthesized $(NiO)_{0.5}$ $(Cr_2O_3)_{0.5}$ nanoparticles, all samples with different calcination temperatures were excited at room temperature at 390 nm. Fig. 6 demonstrates the photoemission spectra of the synthesized $(NiO)_{0.5}$ $(Cr_2O_3)_{0.5}$ nanoparticles with different calcination temperatures. It is apparently seen that broad emission spectra of visible light occurred in the range of 465–550 nm for all samples, which included two peaks associated with emissions at 480 and 527 nm, respectively.

It is well-known that the root cause of visible light emission in oxide nanomaterials is the existence of oxygen vacancies and intrinsic defects, which are the source of free carriers [63–66]. Thus, origination of the first and second peaks is due to the transition resulting from a recombination of electron-hole pairs between oxygen vacancies and metal ions [61]. The transition for the first and most intense peaks located at 480 nm produced photons of blue-green light, while for the second and less intense peak located at 527 nm photons of green light were produced.

From another perspective, it is noticed that the photoluminescence intensity increased (shown in Table 3) with calcination temperature increases of the synthesized binary nanopowders, implying a betterment in its crystallinity when the sample was exposed to higher calcination temperatures.

Conclusion

In this work, the single step based thermal treatment technique was utilised to synthesise $(NiO)_{0.5}$ $(Cr_2O_3)_{0.5}$ semiconductor nanoparticles. The analyzed XRD patterns revealed the formation of a high purity mixed cubic-hexagonal phase structure at all calcination temperatures. The presence of individual elemental constituents of $(NiO)_{0.5}$ $(Cr_2O_3)_{0.5}$ nanoparticles and corresponding atomic composition ratio were verified from the EDX data analysis. Moreover, the lack of elemental loss shown by comparing the EDX results with initial stoichiometric ratios, is an indication of the effectiveness of this novel technique in the synthesis of binary metal oxides nanoparticles. Furthermore, FTIR results confirmed the purity of $(NiO)_{0.5}$ $(Cr_2O_3)_{0.5}$ nanopowders and disappearance of the organic agent beyond temperature of calcination at 500 °C. From another perspective, the TEM results have confirmed the fact that nanopowders' size can growth as the temperature of calcination also increases. As a result, significant improvement to samples' crystallinity has been achieved. In addition, the control this technique offered over $(NiO)_{0.5}$ $(Cr_2O_3)_{0.5}$ particle sizes, through varying the calcination temperature producing binary semiconductor nanoparticles with multiple band gaps energies, meant that they were suitable for use in solar cell applications.

Author contributions

NMA conceived and designed the experiments; NMA, HMK and MAS performed the experiments; NMA, MHF, MAS and HMK analyzed the data; HMK, AHS, AMG, AAB, ES, WJ and HK, contributed reagents/materials/analysis tools; NMA, MHF and MAS wrote the paper. All authors reviewed the manuscript.

Declaration of Competing Interest

The authors declare that they have no known competing financial interests or personal relationships that could have appeared to influence the work reported in this paper.

Acknowledgments

This work was supported from Research Foundation for Advanced Talents of Dezhou University, China, the Ministry of Higher Education Malaysia with the Grant no. Q.J090000.21A4.00D20 under Universiti Teknologi Malaysia (UTM), Malaysia, FRGS/1/2013/SG06/UPNM/03/1 and Geran Putra Berimpak grant no. 9597200 under Universiti Putra Malaysia (UPM), Malaysia.

References

[1] Li J, Zhang JZ. Optical properties and applications of hybrid semiconductor nanomaterials. Coord Chem Rev 2009;253:3015–41.
[2] Ahn J-H, Kim H-S, Lee KJ, Jeon S, Kang SJ, Sun Y, et al. Heterogeneous three-dimensional electronics by use of printed semiconductor nanomaterials. Science 2006;314:1754–7.
[3] Alswata AA, Ahmad MB, Al-Hada NM, Kamari HM, Hussein MZB, Ibrahim NA. Preparation of zeolite/zinc oxide nanocomposites for toxic metals removal from water. Results Phys 2017;7:723–31.
[4] Al-Hada NM, Kamari HM, Abdullah CAC, Saion E, Shaari AH, Talib ZA, et al. Down-top nanofabrication of binary $(CdO)_x(ZnO)_{1-x}$ nanoparticles and their antibacterial activity. Int J Nanomed 2017;12:8309.
[5] Shkir M, Ganesh V, AlFaify S, Yahia I, Zahran H. Tailoring the linear and nonlinear optical properties of NiO thin films through Cr^{3+} doping. J Mater Sci Mater Electron 2018;29:6446–57.
[6] Arif M, Sanger A, Shkir M, Singh A, Katiyar R. Influence of interparticle interaction on the structural, optical and magnetic properties of NiO nanoparticles. Phys B 2019;552:88–95.
[7] Brisse R, Faddoul R, Bourgeteau T, Tondelier D, Leroy J, Campidelli S, et al. Inkjet printing NiO-based p-type dye-sensitized solar cells. ACS Appl Mater Interfaces 2017;9:2369–77.
[8] Kumar A, Sanger A, Kumar A, Chandra R. Fast response ammonia sensors based on TiO_2 and NiO nanostructured bilayer thin films. RSC Adv 2016;6:77636–43.
[9] Zhang Y, Li Z. Low-temperature fabrication of sol–gel NiO film for optoelectronic devices based on the 'fuel'of urea. Ceram Int 2016;42:6360–8.
[10] Sabouri Z, Akbari A, Hosseini HA, Hashemzadeh A, Darroudi M. Bio-based synthesized NiO nanoparticles and evaluation of their cellular toxicity and wastewater treatment effects. J Mol Struct 2019.
[11] Gao H, Guo J, Li Y, Xie C, Li X, Liu L, et al. Highly selective and sensitive xylene gas sensor fabricated from NiO/$NiCr_2O_4$ pp nanoparticles. Sens Actuators B Chem 2019;284:305–15.
[12] Kamari HM, Al-Hada NM, Baqer AA, Shaari AH, Saion E, Comprehensive study on morphological, structural and optical properties of Cr2O3 nanoparticle and its antibacterial activities, J Mater Sci Mater Electron 1–12.
[13] Choi S-W, Katoch A, Kim J-H, Kim SS. Prominent reducing gas-sensing performances of n-SnO_2 nanowires by local creation of p–n heterojunctions by functionalization with p-Cr_2O_3 nanoparticles. ACS Appl Mater Interfaces 2014;6:17723–9.
[14] Ma H, Xu Y, Rong Z, Cheng X, Gao S, Zhang X, et al. Highly toluene sensing performance based on monodispersed Cr_2O_3 porous microspheres. Sens Actuators B 2012;174:325–31.
[15] Ramesh C, Mohan Kumar K, Latha N, Ragunathan V. Green synthesis of Cr_2O_3 nanoparticles using Tridax procumbens leaf extract and its antibacterial activity on Escherichia coli. Curr Nanosci 2012;8:603–7.
[16] Mariammal R, Ramachandran K, Renganathan B, Sastikumar D. On the enhancement of ethanol sensing by CuO modified SnO_2 nanoparticles using fiber-optic sensor. Sens Actuators B Chem 2012;169:199–207.
[17] Yang H, Tao Q, Zhang X, Tang A, Ouyang J. Solid-state synthesis and electrochemical property of SnO_2/NiO nanomaterials. J Alloys Compd 2008;459:98–102.
[18] Saravanan R, Karthikeyan S, Gupta V, Sekaran G, Narayanan V, Stephen A. Enhanced photocatalytic activity of ZnO/CuO nanocomposite for the degradation of textile dye on visible light illumination. Mater Sci Eng C 2013;33:91–8.
[19] Saleh R, Djaja NF, Prakoso SP. The correlation between magnetic and structural properties of nanocrystalline transition metal-doped ZnO particles prepared by the co-precipitation method. J Alloys Compd 2013;546:48–56.

[20] Gupta J, Ahmed AS. Structural, optical and dielectric properties of pure and chromium (Cr) doped nickel oxide nanoparticles. AIP Conference Proceedings. AIP Publishing; 2018.

[21] Peymanfar R, Khodamoradipoor N. Preparation and characterization of copper chromium oxide nanoparticles using modified sol-gel route and evaluation of their microwave absorption properties. Phys Status Solidi (a) 2019:1900057.

[22] Ştefănescu M, Barbu M, Barvinschi P, Ştefănescu O. The obtaining of $NiCr_2O4$ nanoparticles by unconventional synthesis methods. J Therm Anal Calorim 2013;111:1121–7.

[23] Parada C, Morán E. Microwave-assisted synthesis and magnetic study of nanosized Ni/NiO materials. Chem Mater 2006;18:2719–25.

[24] Jaswal VS, Arora AK, Singh J, Kinger M, Gupta VD. Synthesis and characterization of chromium oxide nanoparticles. Orient J Chem 2014;30:559–66.

[25] Dhas NA, Koltypin Y, Gedanken A. Sonochemical preparation and characterization of ultrafine chromium oxide and manganese oxide powders. Chem Mater 1997;9:3159–63.

[26] Mintz T, Bhargava Y, Thorne S, Chopdekar R, Radmilovic V, Suzuki Y, et al. Electrochemical synthesis of functionalized nickel oxide nanowires. Electrochem Solid-State Lett 2005;8:D26–30.

[27] Jana NR, Chen Y, Peng X. Size-and shape-controlled magnetic (Cr, Mn, Fe Co, Ni) oxide nanocrystals via a simple and general approach. Chem Mater 2004;16:3931–5.

[28] Kohli N, Singh O, Singh RC. Influence of pH on particle size and sensing response of chemically synthesized chromium oxide nanoparticles to alcohols. Sens Actuators B 2011;158:259–64.

[29] Ezhilarasi AA, Vijaya JJ, Kaviyarasu K, Maaza M, Ayeshamariam A, Kennedy LJ. Green synthesis of NiO nanoparticles using Moringa oleifera extract and their biomedical applications: cytotoxicity effect of nanoparticles against HT-29 cancer cells. J Photochem Photobiol B 2016;164:352–60.

[30] Thema F, Manikandan E, Gurib-Fakim A, Maaza M. Single phase Bunsenite NiO nanoparticles green synthesis by Agathosma betulina natural extract. J Alloys Compd 2016;657:655–61.

[31] Vijaya JJ, Jayaprakash N, Kombaiah K, Kaviyarasu K, Kennedy LJ, Ramalingam RJ, et al. Bioreduction potentials of dried root of Zingiber officinale for a simple green synthesis of silver nanoparticles: antibacterial studies. J Photochem Photobiol B 2017;177:62–8.

[32] Khamlich S, Manikandan E, Ngom B, Sithole J, Nemraoui O, Zorkani I, et al. Synthesis, characterization, and growth mechanism of α-Cr_2O_3 monodispersed particles. J Phys Chem Solids 2011;72:714–8.

[33] Sone B, Manikandan E, Gurib-Fakim A, Maaza M. Single-phase α-Cr_2O_3 nanoparticles' green synthesis using Callistemon viminalis' red flower extract. Green Chem Lett Rev 2016;9:85–90.

[34] Aisida SO, Akpa PA, Ahmad I, Zhao T-K, Maaza M, Ezema FI. Bio-inspired encapsulation and functionalization of iron oxide nanoparticles for biomedical applications. Eur Polym J 2019;109371.

[35] Al-Hada NM, Saion EB, Shaari AH, Kamarudin MA, Flaifel MH, Ahmad SH, et al. A facile thermal-treatment route to synthesize the semiconductor CdO nanoparticles and effect of calcination. Mater Sci Semicond Process 2014;26:460–6.

[36] Al-Hada NM, Saion EB, Shaari AH, Kamarudin MA, Flaifel MH, Ahmad SH, et al. A facile thermal-treatment route to synthesize ZnO nanosheets and effect of calcination temperature. PLoS One 2014;9:e103134.

[37] Al-Hada NM, Saion EB, Shaari AH, Kamarudeen MA, Flaifel MH, Gene SA, et al. Structural and morphological properties of cadmium oxide nanoparticles prepared by thermal treatment method. Adv Mater Res Trans Tech Publ 2015:291–4.

[38] Kamari H, Al-Hada N, Saion E, Shaari A, Talib Z, Flaifel M, et al. Calcined solution-based PVP influence on ZnO semiconductor nanoparticle properties. Crystals 2017;7:2.

[39] Al-Hada N, Saion E, Talib Z, Shaari A. The impact of polyvinylpyrrolidone on properties of cadmium oxide semiconductor nanoparticles manufactured by heat treatment technique. Polymers 2016;8:113.

[40] Salem A, Saion E, Al-Hada NM, Kamari HM, Shaari AH, Radiman S. Simple synthesis of ZnSe nanoparticles by thermal treatment and their characterization. Results Phys 2017;7:1175–80.

[41] Salem A, Saion E, Al-Hada NM, Kamari HM, Shaari AH, Abdullah CAC, et al. Synthesis and characterization of CdSe nanoparticles via thermal treatment technique. Results Phys 2017;7:1556–62.

[42] Baqer AA, Matori KA, Al-Hada NM, Shaari AH, Saion E, Chyi JLY. Effect of polyvinylpyrrolidone on cerium oxide nanoparticle characteristics prepared by a facile heat treatment technique. Results Phys 2017;7:611–9.

[43] Al-Hada NM, Kamari HM, Baqer AA, Shaari AH, Saion E. Thermal calcination-based production of SnO_2 nanopowder: an analysis of SnO_2 nanoparticle characteristics and antibacterial activities. Nanomaterials 2018;8:250.

[44] Gene SA, Saion EB, Shaari AH, Kamarudeen MA, Al-Hada NM. Fabrication and characterization of nanospinel $ZnCr_2O_4$ using thermal treatement method. Adv Mater Res 2015;1107:301.

[45] Al-Hada NM, Kamari HM, Shaari AH, Saion E. Fabrication and characterization of manganese-zinc ferrite nanoparticles produced utilizing heat treatment technique. Results Phys 2019.

[46] Al-Hada NM, Halimah MK, Shaari AH, Saion E, Aziz SA, Mustafa IS. Structural and morphological properties of manganese-zinc ferrite nanoparticles prepared by thermal treatment route, solid state phenomena. Trans Tech Publ; 2019. p. 307–13.

[47] Baqer AA, Matori KA, Al-Hada NM, Shaari AH, Saion E, Chyi JLY, et al. Structural and optical properties of cerium oxide nanoparticles prepared by thermal treatment method, solid state phenomena. Trans Tech Publ; 2017. p. 132–7.

[48] Baqer AA, Matori KA, Al-Hada NM, Kamari HM, Shaari AH, Saion E, et al. Copper oxide nanoparticles synthesized by a heat treatment approach with structural, morphological and optical characteristics. J Mater Sci Mater Electron 2018;29:1025–33.

[49] Gene SA, Saion E, Shaari AH, Kamarudin MA, Al-Hada NM, Kharazmi A. Structural, optical, and magnetic characterization of spinel zinc chromite nanocrystallines synthesised by thermal treatment method. J Nanomater 2014;2014.

[50] Al-Hada NM, Saion E, Shaari A, Kamarudin M, Gene SA. The influence of calcination temperature on the formation of zinc oxide nanoparticles by thermal-treatment, applied mechanics and materials. Trans Tech Publ; 2014. p. 181–4.

[51] Midala IH, Kamari HM, Al-Hada NM, Tim CK, Muhamad S, Hamza AM, et al. morphological and optical properties of $(ZnO)_{0.2}(ZrO_2)_{0.8}$ nanoparticles. Appl Phys A 2019;125:668.

[52] Hashem M, Saion E, Al-Hada NM, Kamari HM, Shaari AH, Talib ZA, et al. Fabrication and characterization of semiconductor nickel oxide (NiO) nanoparticles manufactured using a facile thermal treatment. Results Phys 2016;6:1024–30.

[53] Kaviyarasu K, Magdalane CM, Anand K, Manikandan E, Maaza M. Synthesis and characterization studies of MgO: CuO nanocrystals by wet-chemical method. Spectrochim Acta Part A Mol Biomol Spectrosc 2015;142:405–9.

[54] Nuru ZY, Arendse C, Nemutudi R, Nemraoui O, Maaza M. Pt–Al_2O_3 nanocoatings for high temperature concentrated solar thermal power applications. Phys B 2012;407:1634–7.

[55] Flaifel MH, Ahmad SH, Abdullah MH, Al-Asbahi BA. NiZn Ferrite filled thermoplastic natural rubber nanocomposites: effect of low temperature on their magnetic behaviour. Cryogenics 2012;52:523–9.

[56] Cullity BD, Stock SR. Elements of X-ray diffraction. NJ: Prentice Hall Upper Saddle River; 2001.

[57] Mayedwa N, Mongwaketsi N, Khamlich S, Kaviyarasu K, Matinise N, Maaza M. Green synthesis of nickel oxide, palladium and palladium oxide synthesized via Aspalathus linearis natural extracts: physical properties & mechanism of formation. Appl Surf Sci 2018;446:266–72.

[58] Lee PJ, Saion E, Al-Hada NM, Soltani N. A simple up-scalable thermal treatment method for synthesis of ZnO nanoparticles. Metals 2015;5:2383–92.

[59] Zakiyah LB, Saion E, Al-Hada NM, Gharibshahi E, Salem A, Soltani N, et al. Up-scalable synthesis of size-controlled copper ferrite nanocrystals by thermal treatment method. Mater Sci Semicond Process 2015;40:564–9.

[60] Baqer AA, Matori KA, Al-Hada NM, Shaari AH, Kamari HM, Saion E, et al. Synthesis and characterization of binary $(CuO)_{0.6}(CeO_2)_{0.4}$ nanoparticles via a simple heat treatment method. Results Phys 2018;9:471–8.

[61] Al-Hada NM, Saion E, Kamari HM, Flaifel MH, Shaari AH, Talib ZA, et al. morphological and optical behaviour of PVP capped binary $(ZnO)_{0.4}(CdO)_{0.6}$ nanoparticles synthesised by a facile thermal route. Mater Sci Semicond Process 2016;53:56–65.

[62] Morales AE, Mora ES, Pal U. Use of diffuse reflectance spectroscopy for optical characterization of un-supported nanostructures. RMxF 2007;53:18–22.

[63] Usha V, Kalyanaraman S, Thangavel R, Vettumperumal R. Effect of catalysts on the synthesis of CuO nanoparticles: structural and optical properties by sol–gel method. Superlattices Microstruct 2015;86:203–10.

[64] Khenfouch M, Baïtoul M, Maaza M. White photoluminescence from a grown ZnO nanorods/graphene hybrid nanostructure, optical. Materials 2012;34:1320–6.

[65] Sithole J, Ngom BD, Khamlich S, Manikanadan E, Manyala N, Saboungi M, et al. Simonkolleite nano-platelets: synthesis and temperature effect on hydrogen gas sensing properties. Appl Surf Sci 2012;258:7839–43.

[66] Kaviyarasu K, Manikandan E, Nuru Z, Maaza M. Investigation on the structural properties of CeO2 nanofibers via CTAB surfactant. Mater Lett 2015;160:61–3.